Nano Research 2013, 6(7): 525–534
DOI 10.1007/s12274-013-0329-3
Research Article
ISSN 1998-0124
CN 11-5974/O4

Advanced rechargeable lithium-ion batteries based on bendable $ZnCo_2O_4$-urchins-on-carbon-fibers electrodes

Bin Liu[1,2], Xianfu Wang[2], Boyang Liu[2], Qiufan Wang[2], Dongsheng Tan[2], Weifeng Song[2], Xiaojuan Hou[2], Di Chen[2] (✉), and Guozhen Shen[1] (✉)

[1] *State Key Laboratory of Superlattices and Microstructures, Institute of Semiconductors, Chinese Academy of Sciences, Beijing 100083, China*

[2] *Wuhan National Laboratory for Optoelectronics (WNLO) and College of Optical and Electronic Information, Huazhong University of Science and Technology (HUST), Wuhan 430074, China*

Received: 20 April 2013
Revised: 5 May 2013
Accepted: 9 May 2013

KEYWORDS
$ZnCo_2O_4$-urchins-on-carbon-fibers, advanced lithium-ion batteries, flexible/wearable features

ABSTRACT

A novel class of $ZnCo_2O_4$-urchins-on-carbon-fibers matrix has been designed, characterized, and used to fabricate high-performance energy storage devices. We obtained a reversible lithium storage capacity of 1180 mA·h/g even after 100 cycles, demonstrating the highreversible capacity and excellent cycle life of the as-prepared samples. Tested as fast-charging batteries, these electrodes exhibited a considerable capacity of 750 mA·h/g at an exceptionally high rate of 20 C (18 A/g), with an excellent cycle life (as long as 100 cycles), which are the best high-rate results reported at such a high charge/discharge current density for $ZnCo_2O_4$-based anode materials in lithium rechargeable batteries. Such attractive properties may be attributed to the unique structure of the binder-free $ZnCo_2O_4$-urchins-on-carbon-fibers matrix. Full batteries were also developed by combining the $ZnCo_2O_4$ anodes with commercial $LiCoO_2$ cathodes, which showed flexible/wearable and stable features for use as very promising future energy storage units.

1 Introduction

In recent years, there are growing demands for the next-generation lithium-ion batteries (LIBs) with both high energy density and high power performance for renewable energy storage [1–19]. LIBs power a wide range of electronic devices including mobile phones, laptop computers, and electric vehicles, etc. To date, high-power LIBs have proved to be more suitable candidates for potential green applications (hybrid electric vehicles (HEVs), plug-in hybrid electric vehicles (PHEVs), and stationary energy storage) compared to nickel metal hydride, alkaline, and lead–acid batteries because of their higher volumetric and gravimetric energy density. However, commercially available LIBs usually use graphite anodes, which have a quite low

Address correspondence to Guozhen Shen, gzshen@semi.ac.cn; Di Chen, dichen@mail.hust.edu.cn

theoretical capacity of only 372 mA·h/g and relatively poor rate capability [20]. Since the currently LIBs cannot satisfy the demands of future high-performance battery units, it remains as a significant challenge to achieve high-power storage devices with greatly improved energy and power densities.

To meet the requirements of future fast energy conversion and consumption devices, one strategy is to find alternative anode materials with enhanced rate capabilities and better sustainable power delivery [21–25]. In particular, $ZnCo_2O_4$ is an excellent candidate as an anode material due to its high reversible capacity, long cycling life, and environmental friendliness [26–31]. Various approaches have been developed to synthesize $ZnCo_2O_4$ nanostructures—including nanoparticles, nanotubes and nanowires—in an effort to improve their performance. However, the low conductivity of $ZnCo_2O_4$ active materials leads to excess performance degradation when charging/discharging at high current densities. Hence, there is still room to improve the rate capabilities of $ZnCo_2O_4$ anodes to satisfy the needs of high-power energy storage systems with high energy and power densities.

Herein, we report the fabrication of high-power LIBs with self-assembled $ZnCo_2O_4$ urchins on carbon fibers as the binder-free anodes, which were prepared by growing $ZnCo_2O_4$ urchins on textured carbon fibers. A reversible capacity of as high as 1,180 mA·h/g even after 100 cycles was obtained, demonstrating the high reversible capacity and excellent cycle life of as-prepared anodes. Surprisingly, the as-synthesized anode electrode showed an exceptionally high rate of 20 C (18 A/g) with the high capacity of 750 mA·h/g, which is much better than the best value reported for $ZnCo_2O_4$-based anodes. The as-prepared $ZnCo_2O_4$ urchins-on-carbon-fibers composites were also fabricated into highly flexible and stable full batteries in order to demonstrate their practical applications in flexible/portable electronics.

2 Experimental

2.1 Synthesis of $ZnCo_2O_4$ urchins-on-carbon-fibers composites

In a typical process, 0.6 g of zinc nitrate, 1.2 g of cobalt nitrate, 0.6 g of urea, and a given amount of distilled water were mixed step-by-step under vigorous stirring. The mixture became a homogeneous solution with a pink color, and then was transferred into a Teflon-lined stainless steel autoclave with a volume of 60 mL. A piece of cleaned carbon fiber cloth was placed into Teflon-lined stainless, and the vessel was heated in an electric oven at 200 ℃ for 12 h. After the autoclave was cooled naturally to room temperature, the samples were collected and washed for at least three cycles using deionized water, and then vacuum dried at 60 ℃. Afterwards, thermal treatment of the as-synthesized samples was performed at 400 ℃ for 2 h.

2.2 Characterization of the samples

X-ray diffraction (XRD, X' Pert PRO, PANalytical B. V.) with radiation from a Cu target (Kα, λ = 0.15406 nm), field emission scanning electron microscopy (FESEM, JEOL JSM-6700F, 5 kV), and high-resolution transmission electron microscopy (HRTEM, Tecnai G2 20) were employed to characterize the as-fabricated samples.

2.3 Battery assembly and electrochemical characterization

Electrochemical experiments were performed using CR2032-type coin cells with Celgard 2400 as separator and lithium-foil as counter electrode. A piece of 3D self-assembled $ZnCo_2O_4$ urchins-on-carbon-fibers electrode was used directly as the working electrode without the addition of any other ancillary materials (binder or carbon black). Both the carbon fiber cloth with loaded sample and carbon fiber cloth were weighed on a high-precision analytical balance (Sartorius, max weight 5,100 mg, d = 0.001 mg). The reading difference was the exact mass of the sample coated on the carbon fibers. The loading density of the $ZnCo_2O_4$ active materials was calculated as 2.2–3.6 mg/cm^2. The electrolyte was 1 M $LiPF_6$ in a mixture of ethylene carbonate (EC) and diethyl carbonate (DEC) (1:1 ratio by volume). The cells were assembled in an argon-filled glovebox where water and oxygen concentrations were limited to below 1 ppm. CR2032-type coin cells were tested at various C-rates (1 C corresponding to about 900 mA·h/g with respect to the anode mass) in the voltage window of 0.01–3.0 V (vs. Li^+/Li) on a

LAND Battery Testing System. Similarly, fully flexible lithium-ion batteries were assembled by sandwiching a Celgard 2400 membrane between a $ZnCo_2O_4$ urchins-on-carbon-fibers anode and a $LiCoO_2$ cathode. The mass of the $ZnCo_2O_4$ samples was calculated to be around 18–20 mg, and the loading density of the $ZnCo_2O_4$ active materials was 1.6–1.8 mg/cm^2. An aqueous solution of 1.05 M $LiPF_6$ in ethylene carbonate/diethyl carbonate (DMC) (1:1 ratio by volume) served as the electrolyte. The whole assembly was packaged in a flexible plastic bag. The electrochemical measurement of these electrodes was performed on the LAND Battery Testing System. The electrochemical tests were performed between 2.2–3.7 V for complete anode-limited flexible Li-ion batteries at 1 C with respect to the anode mass on the LAND Battery Testing System.

3 Results and discussion

3.1 Synthesis and structural characterization

$ZnCo_2O_4$ urchins were grown on textured carbon fiber cloth via a conventional hydrothermal approach by using 2 mmol of Zn^{2+} and 4 mmol of Co^{2+} source materials. By putting textured carbon fiber cloth into the reaction system, urchin-like $ZnCo_2O_4$ arrays, composed of radially-aligned nanowires, were found deposited on the cloth with very high density (Fig. 1(a)). During this process, it should be mentioned that the concentration of the source materials plays a key role in determining the morphology of the product. Using the concentration of Zn^{2+} as an example, only $ZnCo_2O_4$ urchins were grown under the conditions of Zn^{2+} source materials with concentrations higher than 2 mmol, whilst concentrations lower than 2 mmol resulted in the formation of aligned $ZnCo_2O_4$ nanowire arrays, as shown in our previous report [31]. We also found that a Zn^{2+} concentration higher than 2 mmol is not good for another reason, since too many urchins were grown on carbon fibers at higher concentration. Urchins with too high a density resulted in the detachment of the active materials during the subsequent electrochemical reaction, leading to a rapid decrease of the capacity of the LIBs. It is well known that during a hydrothermal process, source materials with higher concentration favor the formation of more seeds in the initial state, which act as the deposition sites for the subsequent material growth. With prolonging of the reaction time, more source species are adsorbed on the seeds and the extremely high ion concentrations resulted in the formation of urchins instead of nanowires due to the surface site limit of the carbon fiber. Figure 1(b) shows optical images of the carbon fiber cloths before and after $ZnCo_2O_4$ growth. The obvious color change and the final uniform color of the cloth indicate the uniform coating of $ZnCo_2O_4$ samples. Figures 1(c) and 1(d) show photographic images of a bent carbon fiber cloth coated with $ZnCo_2O_4$, revealing it still keeps a highly flexible/stretchable nature.

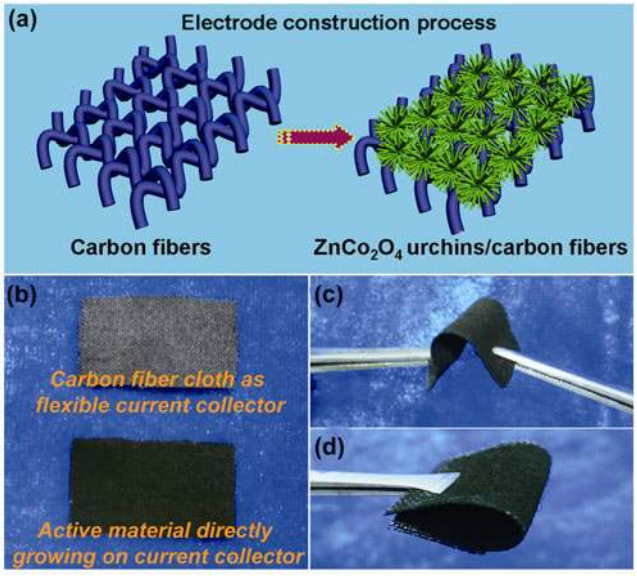

Figure 1 (a) Construction process of $ZnCo_2O_4$-based electrodes by using a hydrothermal method. (b) Photographs of the commercial carbon fibers before and after coating with active materials. (c) and (d) The as-synthesized electrodes under bending.

Figure 2(a) shows a SEM image of the as-synthesized product, where we can see that the carbon fibers with smooth surfaces (Fig. S1 in the Electronic Supplementary Material (ESM)) were uniformly coated with high-density samples. The higher magnification SEM images depicted in Figs. 2(b) and 2(c) reveal that the samples actually have an urchin-like morphology. Each urchin has a diameter of approximately 25 μm with numerous nanowires growing out radially from the center of the urchin. Figure 2(d) is a SEM image of a single urchin, where the radially-grown nanowires were found to have diameters of about 80–100 nm.

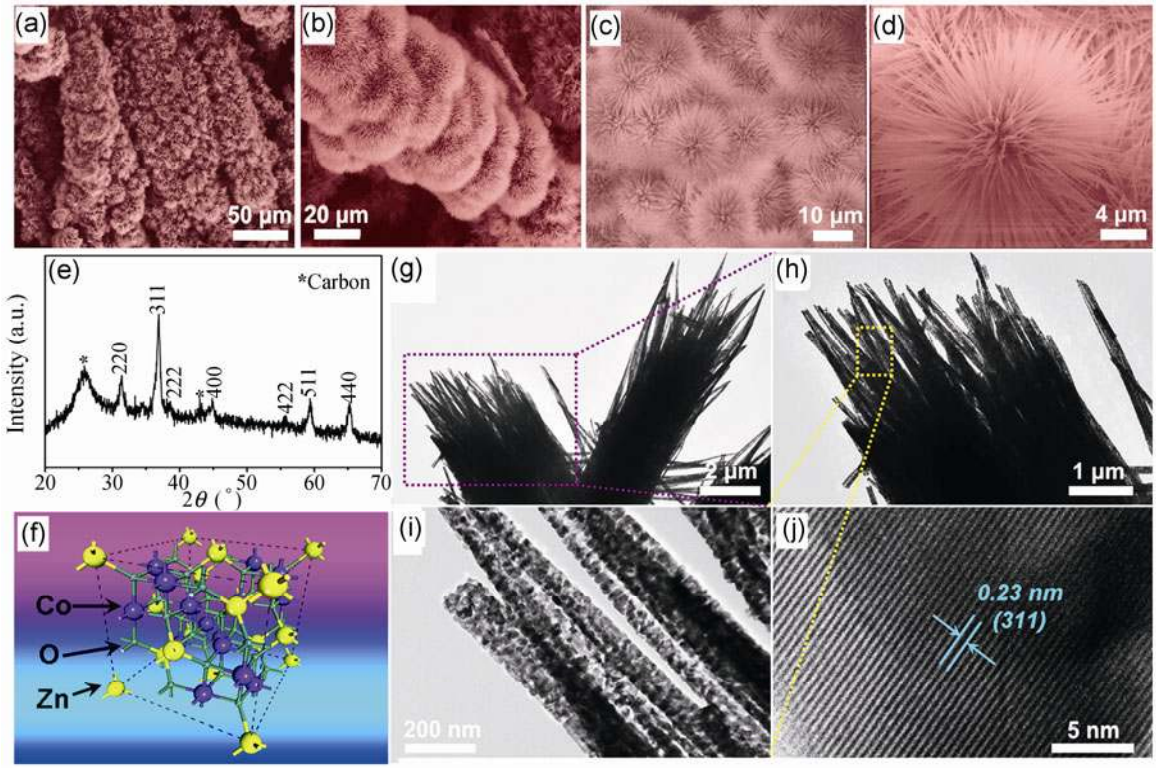

Figure 2 (a)–(d) FESEM images, and (e) XRD pattern of the synthesized $ZnCo_2O_4$ urchins grown on carbon fibers. (f) Schematic illustration of the crystal structure of $ZnCo_2O_4$. (g)–(i) TEM images and (j) HRTEM image of the $ZnCo_2O_4$ urchins.

Figure 2(e) shows the XRD pattern of the as-synthesized product, confirming the formation of pure spinel $ZnCo_2O_4$ (JCPDS Card No. 23-1390). The crystal structure of spinel $ZnCo_2O_4$ is demonstrated in Fig. 2(f). The yellow, purple, and green spheres represent Zn, Co, and O atoms, respectively. Further information about the $ZnCo_2O_4$ urchins was obtained transmission electron microscopy (TEM). Figures 2(g) and 2(h) are TEM images taken from the as-synthesized $ZnCo_2O_4$ urchins, where radially grown nanowires can be easily seen protruding from the center of an urchin. The higher magnification TEM image shown in Fig. 2(i) reveals that typical $ZnCo_2O_4$ nanowires with diameters of about 80–100 nm have porous structures and are composed of numerous small nanocrystals. Figure 2(j) is a HRTEM image taken from a single porous nanowire. The clearly resolved lattice fringe spacing was calculated to be about 0.23 nm, corresponding to the (311) planes of spinel $ZnCo_2O_4$.

3.2 Electrochemical characterization

To investigate the electrochemical performance of the as-synthesized $ZnCo_2O_4$ urchins grown on carbon fibers, they were configured as CR2032-type coin cells. Galvanostatic charge/discharge tests were performed to investigate the lithium insertion/extraction behavior. Figures 3(a) and 3(b) show the voltage profiles of the $ZnCo_2O_4$-based electrodes for the 1st, 2nd, 10th, and 100th charge/discharge cycles in a voltage window of 0.01–3.0 V at the rates of 0.2 C and 5 C (1 C = 900 mA·h/g), respectively. From the voltage profiles, it can be seen that all discharge curves exhibit distinct plateaus between 1.0 and 1.2 V. The discharge capacities for the first cycle at 0.2 and 5 C are 1,310 and 1,350 mA·h/g, respectively, higher than the theoretical capacity for $ZnCo_2O_4$ (900 mA·h/g). According to previous reports, this can be attributed to the irreversible reactions which are commonly observed for such anode materials [26, 28, 30–32]. After the 1st cycle, the following charge/discharge curves tended to be stable, illustrating the electrochemical reactions have gradually proceeded into the cycle stages [32]. Figure 3(c) shows the cycling performance at 0.2 C rate for the $ZnCo_2O_4$-based electrodes. The curves clearly reveal

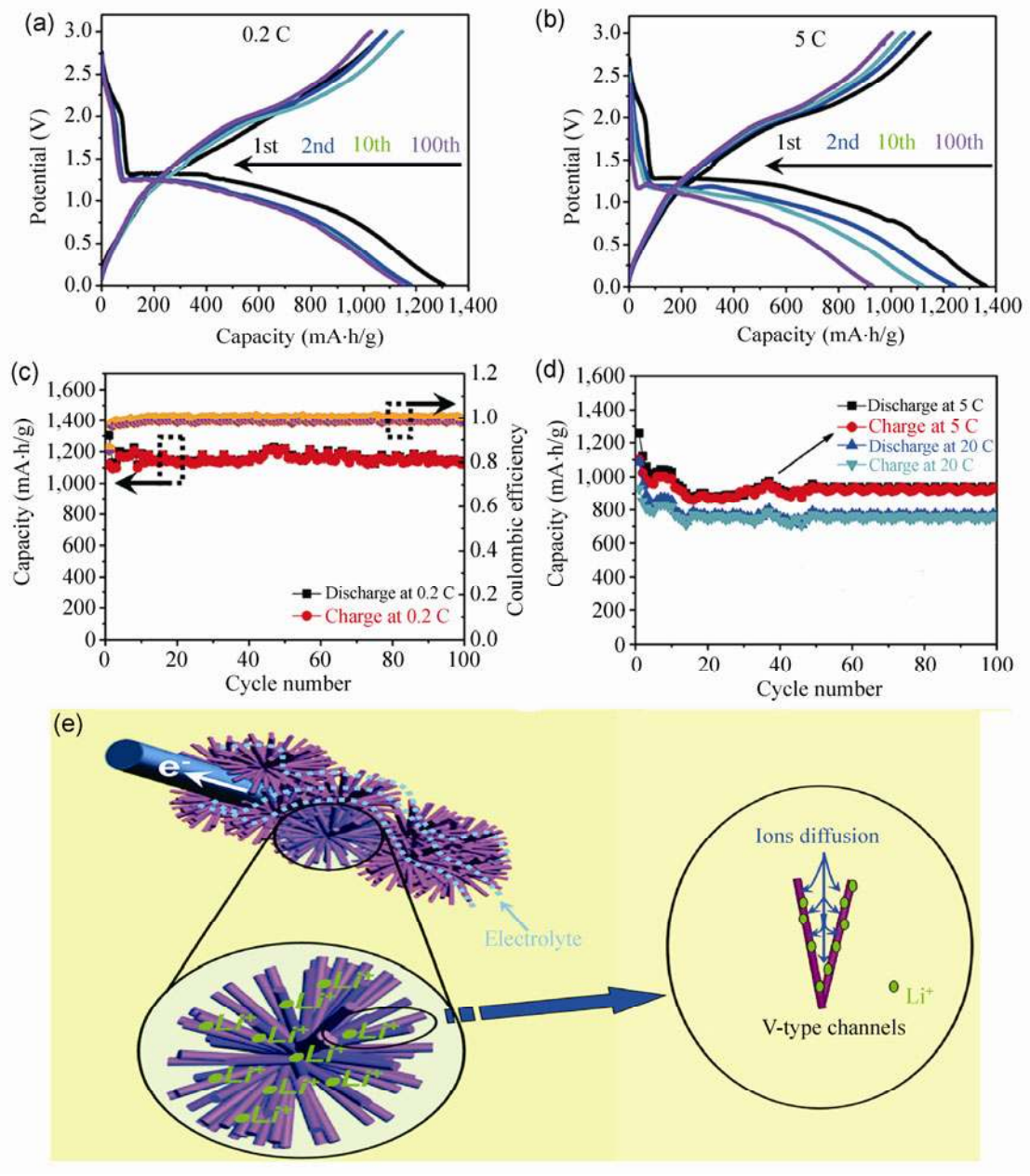

Figure 3 Discharge/charge profiles of the $ZnCo_2O_4$-urchins-on-carbon-fibers electrodes at the current densities of (a) 0.2 ˚C and (b) 5 ˚C. (c) Cycling performance of the electrodes at 0.2 ˚C over 100 cycles and their corresponding columbic efficiency (CE). (d) Charge/discharge capacities vs. cycle number for the electrodes at the high rates of 5 ˚C and 20 ˚C over 100 cycles. (e) Schematic illustration of the operating principles of a rechargeable lithium-ion battery based on the $ZnCo_2O_4$ electrodes.

that the as-synthesized $ZnCo_2O_4$-based electrodes delivered improved reversible discharge capacity at 0.2 C and the capacity still remains at 1,180 mA·h/g even after 100 cycles, demonstrating the high reversible capacity and excellent cycle life. Figure S2 (in the ESM) shows the SEM image of the samples cycled at 0.2 C after 50 cycles. From the image, we can see that although some cracks were observed for the electrodes, the urchin-like structures were still retained quite well, further proving the stability of the electrodes after cycling tests. Since the contribution of the carbon fibers to the capacity is negligible (Fig. S3 in the ESM), the total capacity is primarily attributed to the capacity of the loaded active $ZnCo_2O_4$ material. In addition,

the columbic efficiency between the discharge and the charge capacities of the samples at 0.2 C is higher than 98%, indicating excellent electrochemical reversibility during the lithium insertion and extraction reactions.

The rate capability of the $ZnCo_2O_4$-based electrode was further studied by imposing higher discharge rates. Figure 3(d) shows the discharge capacities versus cycle number at the high rates of 5 C (4.5 A/g) and 20 C (18 A/g) in the voltage window of 0.01–3 V. At a rate of 5 C, the reversible discharge capacity still reached up to approximately 900 mA·h/g, which is much larger than that of commercially used graphite (372 mA·h/g) even at the high current density. Surprisingly, an exceptional high specific capacity was obtained for the current $ZnCo_2O_4$-based electrode even at a high rate of 20 C. As shown in Fig. 3(d), a specific capacity of as high as 750 mA·h/g was obtained at 20 C (18 A/g) over 100 cycles. The value still retained 83.3% of the theoretical capacity for $ZnCo_2O_4$ active materials. To date, this is the best high-rate result reported under such high charge/discharge current densities without the addition of any other ancillary materials (carbon black or binder) for $ZnCo_2O_4$ anode materials in lithium rechargeable batteries. This shows that the $ZnCo_2O_4$-urchins-on-carbon-fibers electrodes are promising candidates for various potential applications, such as electric vehicles (EV), HEV, and flexible/portable electronic devices.

3.3 Analysis of electrode-matrix merits

The operating principles of the $ZnCo_2O_4$-urchins-on-carbon-fibers electrodes are shown in Fig. 3(e). By virtue of their structural features, urchin-like structures can yield more "V-type" channels than randomly distributed nanowires or aligned nanowire arrays, which facilitate ion/electron transport inside active materials, diffusion of the electrolyte, and sufficient contact area between the electrolyte and the active electrodes in a short time for fast energy storage according to previous reports [31, 33, 34]. Besides, for the current $ZnCo_2O_4$-urchins-on-carbon-fibers electrodes, $ZnCo_2O_4$ urchins were found grown tightly on the highly conductive carbon fibers, which are beneficial to the insertion/extraction of Li^+ because of the very good adhesion and electrical contact between them, and also shorten the charge transfer pathway and lower the exchange resistance for lithium ions between active functional materials and electrolyte [32–38], thus enhance the rate capability of these electrodes to a large extent. All the above effects will undoubtedly make it possible to achieve the observed high rate capability and excellent cycling stability of the $ZnCo_2O_4$ electrodes with their unique urchin-like architecture.

3.4 Stability and flexibility measurements

Recently, flexible electronics has received increasing attention because it enables new classes of future applications, such as flexible displays, electronic textiles, and many other portable consumer electronic devices. Even though current developments in rechargeable batteries have moved towards thinner, lighter, and cheaper solutions, numerous existing energy-harvesting/storage devices are still too bulky, heavy, and inflexible for flexible electronics applications. As we demonstrated above (Fig. 1), the as-grown $ZnCo_2O_4$-urchins-on-carbon-fibers have excellent flexibility, which makes them suitable candidates for flexible electronics. In this part, we demonstrate the fabrication of highly flexible full batteries by using the as-grown $ZnCo_2O_4$/carbon composite electrode as a binder-free anode. Figure S4 (in the ESM) displays a schematic illustration of the assembly of a flexible thin full battery with a thickness of about 0.6 mm. The battery consists of $LiCoO_2$/Al foil (cathode), separator, liquid electrolyte, $ZnCo_2O_4$ urchins-on-carbon-fibers (anode), and aluminum–plastic film. In the full battery, the capacity of the commercial $LiCoO_2$ cathode (~40 mA·h) is much higher than the total capacity of the $ZnCo_2O_4$ active materials (about 18 mA·h). This means that the full batteries are anode-limited and the specific capacity and rate of the batteries refer to the mass of the loaded $ZnCo_2O_4$ electrodes [31, 39, 40]. Figure 4(a) shows the cycling performance of the flexible full battery in the voltage window 2.2–3.7 V at 0.2 C, showing a reversible capacity value of 1,172 mA·h/g after 50 cycles with a coulombic efficiency of approximately 99%, further confirming the excellent electrochemical performance of the as-fabricated $ZnCo_2O_4$-urchins-on-carbon-fibers electrodes. To further demonstrate the flexibility and

stability of the flexible full battery, we checked the performance of the flexible device by bending it with different bending angles and bending cycles. Figures 4(b) and 4(c) show the corresponding results after proceeding with 50 cycles as shown in Fig. 4(a). From Fig. 4(b), we can see that the reversible capacity of the flexible device remains almost when the device was bent by 30°, 60°, 90°, 120°, or 180°. Moreover, Fig. 4(c) illustrates that the capacity of the devices after being bent for different numbers of cycles (50, 100, 150, 200, and 250 cycles), also remains almost constant. These results indicate the high flexibility, good folding strength, and electrical stability of the as-assembled flexible energy storage devices. Figure 4(d) shows the corresponding potential profiles of the full battery for its 1st, 2nd, 10th, and 50th galvanostatic charge/discharge cycles in the voltage window of 2.2–3.7 V at the rate of 0.2 C. The initial irreversible discharge capacity of the electrodes is about 1,175 mA·h/g and the reversible discharge capacity remains stable in the following cycles, indicating good reversibility and good matching characteristics between the anode and cathode electrodes in the complete battery system. To further investigate to the rate capability of our samples, the various rates were increased from 0.1 C for 10 cycles, stepwise to 0.2 C for 10 cycles, 2 C for 10 cycles, 5 C for 10 cycles, then back to 0.1 C for 10 cycles; the corresponding specific capacity loss was negligible, as shown in Fig. 4(e). Thus, these electrodes exhibit a high rate performance in the full batteries even at very fast lithium ion insertion–extraction speed, which is in agreement with the excellent rate results of the above half-cells based on these $ZnCo_2O_4$ electrodes. Self-discharge property is a very important parameter for energy storage devices. The self-discharge property of the flexible full battery was studied and the corresponding result is demonstrated in Fig. 4(f), which shows the potential profile of the flexible full battery up to 680 h. From the plot, it can be seen that the average potential remains almost 2.75 V over 680 h, indicating extremely low self-discharging rate and steady electrical capability.

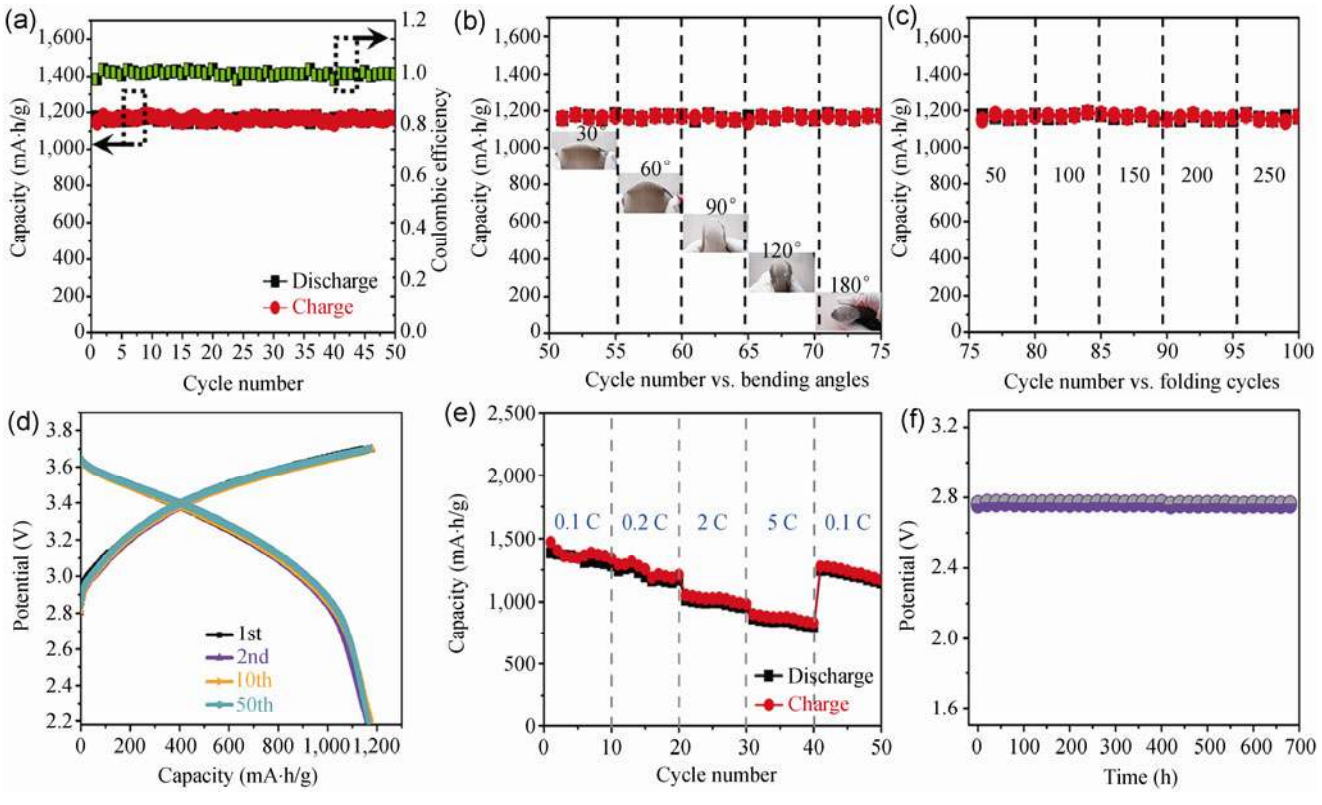

Figure 4 (a) Cycling performance and the corresponding coulombic efficiency; capacity variation as a function of (b) bending angle and (c) number of folding cycles; (d) the corresponding voltage profiles; (e) the rate performance at various current densities; (f) self-discharging characteristics of as-assembled flexible full battery based on $ZnCo_2O_4$ urchins-on-carbon-fibers composite electrodes.

3.5 Feasibility of devices

With the features of excellent flexibility, stable and ultra-high electrochemical performance, and ultra-thin thickness, the as-fabricated energy storage devices could, in principle, be integrated with clothes or bags for practical flexible/portable potential applications. Figure 5(a) shows a photograph of a flexible full battery integrated on a T-shirt, which can easily light a commercial light-emitting diode (LED). The performance did not show any degradation even when the device was transferred onto the curved sleeve of clothes, as shown in Fig. 5(b). Similar results were also obtained when integrating the flexible full battery into a travel bag, as shown in Figs. 5(c) and 5(d). This confirms that the flexible battery can be easily integrated to meet the increasing requirements of future wearable/portable energy storage devices by virtue of its features of space saving (ultra-light/ultra-thin properties), maximized flexibility (transferability and wearable devices), and excellent mechanical stability under bending. Figure 5(e) shows four lighting Nixie tubes powered by the flexible battery, making up a pattern of "HUST", the logo of Huazhong University of Science and Technology. It should be noted that the brightness of the Nixie tubes is hardly affected by external bending stress, further confirming the good electrical stability of the fabricated flexible battery.

Figure 5 (a)–(d) Optical images of a flexible/ultra-thin Li-ion battery transferred onto daily clothes and travel bag, showing its future wide wearable/portable electronic applications. (e) A flexible lithium-ion battery lighting four Nixie tubes, showing the logo of "HUST".

4 Conclusions

Advanced rechargeable LIBs have been successfully fabricated by using hydrothermally synthesized $ZnCo_2O_4$-urchins-on-carbon-fibers structures as the binder-free anodes. An extremely high capacity of 750 mA·h/g was obtained at very high charging rate of 18,000 mA/g (20 C), which corresponds to 83.3% of the theoretical capacity for $ZnCo_2O_4$ active materials. A highly flexible full battery was also fabricated with good electrical stability under fully mechanical bending. This can be easily integrated with clothes or bags to meet the requirements for daily uses. Our strategy here makes it possible to directly assemble high-power LIBs by designing new nanostructured electrodes. Besides, fully flexible devices also allow the material to be directly applied in various fields, such as wearable/stretchable electronic devices, high-power sustainable vehicles, and next-generation flexible energy storage devices.

Acknowledgements

This work was supported by the National Natural Science Foundation of China (Nos. 51002059, 21001046, 91123008), the Major State Basic Research Development Program of China (973 Program, No. 2011CB933300), the Program for New Century Excellent Talents of the University in China (grant No. NCET-11-0179) and the Natural Science Foundation of Hubei Province (No. 2011CDB035). Special thanks to the Analytical and Testing Center of HUST and the Center of Micro-Fabrication and Characterization (CMFC) of WNLO for using their facilities.

Electronic Supplementary Material: SEM image of carbon fibers, electrochemical tests of carbon fibers, and schematic illustration of the assembly procedure of the full battery system is available in the online version of this article at http://dx.doi.org/10.1007/s12274-013-0329-3.

References

[1] Scrosati, B. Paper powers battery breakthrough. *Nat. Nanotechnol.* **2007**, *2*, 598–599.

[2] Poizot, P.; Laruelle, S.; Grugeon, S.; Dupont, L.; Tarascon, J. M. Nano-sized transition-metal oxides as negative-electrode materials for lithium-ion batteries. *Nature* **2000**, *407*, 496–499.

[3] Wang, H. L.; Yang, Y.; Liang, Y. Y.; Robinson, J. T.; Li, Y. G.; Jackson, A.; Cui, Y.; Dai, H. J. Graphene-wrapped sulfur particles as rechargeable lithium–sulfur battery cathode material with high capacity and cycling stability. *Nano Lett.* **2011**, *11*, 2644–2647.

[4] Lu, J.; Nan, C. Y.; Li, L. H.; Peng, Q.; Li, Y. D. Flexible SnS nanobelts: Facile synthesis, formation mechanism and application in Li-ion batteries. *Nano Res.* **2013**, *6*, 55–64.

[5] Seng, K. H.; Park, M. H.; Guo, Z. P.; Liu, H. K.; Cho, J. Self-assembled germanium/carbon nanostructures as high-power anode material for the lithium-ion battery. *Angew. Chem. Int. Ed.* **2012**, *51*, 5657–5661.

[6] Xiao, X. L.; Lu, J.; Li, Y. D. $LiMn_2O_4$ microspheres: Synthesis, characterization and use as a cathode in lithium ion batteries. *Nano Res.* **2010**, *3*, 733–737.

[7] Yang, Y.; Jeong, S.; Hu, L. B.; Wu, H.; Lee, S. W.; Cui, Y. Transparent lithium-ion batteries. *Proc. Natl. Acad. Sci. U.S.A.* **2011**, *108*, 13013–13018.

[8] Chen, H. T.; Xu, J.; Chen, P. C.; Fang, X.; Qiu, J.; Fu, Y.; Zhou, C. W. Bulk synthesis of crystalline and crystalline core/amorphous shell silicon nanowires and their application for energy storage. *ACS Nano* **2011**, *5*, 8383–8390.

[9] Guo, Y. G.; Hu, J. S.; Wan, L. J. Nanostructured materials for electrochemical energy conversion and storage devices. *Adv. Mater.* **2008**, *20*, 2878–2887.

[10] Cao, F. F.; Deng, J. W.; Xin, S.; Ji, H. X.; Schmidt, O. G.; Wan, L. J.; Guo, Y. G. Cu–Si nanocable arrays as high-rate anode materials for lithium-ion batteries. *Adv. Mater.* **2011**, *23*, 4415–4420.

[11] Magasinski, A.; Dixon, P.; Hertzberg, B.; Kvit, A.; Ayala, J.; Yushin, G. High-performance lithium-ion anodes using a hierarchical bottom-up approach. *Nat. Mater.* **2010**, *9*, 353–358.

[12] Wang, Z. Y.; Zhou, L.; Lou, X. W. Metal oxide hollow nanostructures for lithium-ion batteries. *Adv. Mater.* **2012**, *24*, 1903–1911.

[13] Lou, X. W.; Deng, D.; Lee, J. Y.; Feng, J.; Archer, L. A. Self-supported formation of needle-like Co_3O_4 nanotubes and their application as lithium-ion batteries electrodes. *Adv. Mater.* **2008**, *20*, 258–262.

[14] Wei, J.; Yue, Q.; Sun, Z. K.; Deng, Y. H.; Zhao, D. Y. Synthesis of dual-mesoporous silica using non-ionic diblock copolymer and cationic surfactant as co-templates. *Angew. Chem. Int. Ed.* **2012**, *51*, 6149–6153.

[15] Ishikawa, F. N.; Chang, H. K.; Ryu, K.; Chen, P. C.; Badmaev, A.; De Arco, L. G.; Shen, G. Z.; Zhou, C. W. *ACS Nano* **2009**, *3*, 73–79.

[16] Liu, B.; Wang, X. F.; Chen, H. T.; Wang, Z. R.; Chen, D.; Cheng, Y. B.; Zhou, C. W.; Shen, G. Z. Hierarchical silicon nanowires–carbon textiles matrix as a binder-free anode for high-performance advanced lithium-ion batteries. *Sci. Rep.* **2013**, *3*, 1622.

[17] Wang, Z. R.; Wang, H.; Liu, B.; Qiu, W. Z.; Zhang, J.; Ran, S. H.; Huang, H. T.; Xu, J.; Han, H. W.; Chen, D.; Shen, G. Z. Highly ordered TiO_2 macropore arrays as transparent photocatalysts. *ACS Nano* **2011**, *5*, 8412–8419.

[18] Liu, B.; Wang, Z. R.; Dong, Y.; Zhu, Y. G.; Gong, Y.; Ran, S. H.; Liu, Z.; Xu, J.; Xie, Z.; Chen, D.; Shen, G. Z. ZnO-nanoparticle-assembled cloth for flexible photodetectors and recyclable photocatalysts. *J. Mater. Chem.* **2012**, *22*, 9379–9384.

[19] Tripathi, R.; Ramesh, T. N.; Ellis, B. L.; Nazar, L. F. Scalable synthesis of tavorite $LiFeSO_4F$ and $NaFeSO_4F$ cathode materials. *Angew. Chem. Int. Ed.* **2010**, *49*, 8738–8742.

[20] Hossain, S.; Kim, Y. K.; Saleh, Y.; Loutfy, R. Comparative studies of MCMB and C/C composite as anodes for lithium-ion battery systems. *J. Power Sources* **2003**, *114*, 264–276.

[21] Wang, G. X.; Liu, H.; Liu, J.; Qiao, S. Z.; Lu, G. M.; Munroe, P.; Ahn, H. Mesoporous $LiFePO_4$/C nanocomposite cathode materials for high power lithium ion batteries with superior performance. *Adv. Mater.* **2010**, *22*, 4944–4948.

[22] Doherty, C. M.; Caruso, R. A.; Smarsly, B. M.; Adelhelm, P.; Drummond, C. J. Hierarchically porous monolithic $LiFePO_4$/carbon composite electrode materials for high power lithium ion batteries. *Chem. Mater.* **2009**, *21*, 5300–5306.

[23] Luo, J. Y.; Xia, Y. Y. Aqueous lithium-ion battery $LiTi_2(PO_4)_3/LiMn_2O_4$ with high power and energy densities as well as superior cycling stability. *Adv. Funct. Mater.* **2007**, *17*, 3877–3884.

[24] Wu, X. L.; Jiang, L. Y.; Cao, F. F.; Guo, Y. G.; Wan, L. J. $LiFePO_4$ nanoparticles embedded in a nanoporous carbon matrix: Superior cathode material for electrochemical energy-storage devices. *Adv. Mater.* **2009**, *21*, 2710–2714.

[25] Chen, J. S.; Lou, X. W. SnO_2-based nanomaterials: Synthesis and application in lithium-ion batteries. *Small*, in press, DOI: 10.1002/smll.201202601.

[26] Sharma, Y.; Sharma, N.; Rao, G.; Chowdari, B. Nanophase $ZnCo_2O_4$ as a high performance anode material for Li-ion batteries. *Adv. Funct. Mater.* **2007**, *17*, 2855–2861.

[27] Deng, D.; Lee, J. Y. Linker-free 3D assembly of nanocrystals with tunable unit size for reversible lithium ion storage. *Nanotechnology* **2011**, *22*, 355401.

[28] Hu, L. L.; Qu, B. H.; Li, C. C.; Chen, Y. J.; Mei, L.; Lei, D. N.; Chen, L. B.; Li, Q. H.; Wang, T. H. Facile synthesis of uniform mesoporous $ZnCo_2O_4$ microspheres as a high-performance anode material for Li-ion batteries. *J. Mater. Chem. A* **2013**, *1*, 5596–5602.

[29] Qiu, Y. C.; Yang, S. H.; Deng, H.; Jin, L. M.; Li, W. S. A novel nanostructured spinel $ZnCo_2O_4$ electrode material:

Morphology conserved transformation from a hexagonal shaped nanodisk precursor and application in lithium ion batteries. *J. Mater. Chem.* **2010**, *20*, 4439–4444.

[30] Du, N.; Xu, Y. F.; Zhang, H.; Yu, J. X.; Zhai, C. X.; Yang, D. R. Porous $ZnCo_2O_4$ nanowires synthesis via sacrificial templates: High-performance anode material of Li-ion batteries. *Inorg. Chem.* **2011**, *50*, 3320–3324.

[31] Liu, B.; Zhang, J.; Wang, X. F.; Chen, G.; Chen, D.; Zhou, C. W.; Shen, G. Z. Hierarchical three-dimensional $ZnCo_2O_4$ nanowire arrays/carbon cloth anodes for a novel class of high-performance flexible lithium-ion batteries. *Nano Lett.* **2012**, *12*, 3005–3011.

[32] Wang, Y.; Zhang, H. J.; Lu, L.; Stubbs, L. P.; Wong, C. C.; Lin. J. Y. Designed functional systems from peapod-like Co@carbon to Co_3O_4@carbon nanocomposites. *ACS Nano* **2010**, *4*, 4753–4761.

[33] Wang, Y. G.; Li, H. Q.; Xia, Y. Y. Ordered whiskerlike polyaniline grown on the surface of mesoporous carbon and its electrochemical capacitance performance. *Adv. Mater.* **2006**, *18*, 2619–2623.

[34] Yuan, C. Z.; Zhang, X. G.; Hou, L. R.; Shen, L. F.; Li, D. K.; Zhang, F.; Fan, C. G.; Li, J. M. Lysine-assisted hydrothermal synthesis of urchin-like order arrays of mesoporous $Co(OH)_2$ nanowires and their application in electrochemical capacitors. *J. Mater. Chem.* **2010**, *20*, 10809–10816.

[35] Li, B. X.; Rong, G. X.; Xie, Y.; Huang, L. F.; Feng, C. Q. Low-temperature synthesis of α-MnO_2 hollow urchins and their application in rechargeable Li^+ batteries. *Inorg. Chem.* **2006**, *45*, 6404–6410.

[36] Xu, M. W.; Kong, L. B.; Zhou, W. J.; Li, H. L. Hydrothermal synthesis and pseudocapacitance properties of α-MnO_2 hollow spheres and hollow urchins. *J. Phys. Chem. C* **2007**, *111*, 19141–19147.

[37] Han, C. H.; Pi, Y. Q.; An, Q. Y.; Mai, L. Q.; Xie, J. L.; Xu, X.; Xu, L.; Zhao, Y. L.; Niu, C. J.; Khan, A. M.; He, X. Y. Substrate-assisted self-organization of radial β-$AgVO_3$ nanowire clusters for high rate rechargeable lithium batteries. *Nano Lett.* **2012**, *12*, 4668–4673.

[38] Nam, K. T.; Kim, D. W.; Yoo, P. J.; Chiang, C. Y.; Meethong, N.; Hammond, P. T.; Chiang, Y. M.; Belcher, A. M. Virus-enabled synthesis and addembly of nanowires for lithium ion battery electrodes. *Science* **2006**, *312*, 885–888.

[39] Armstrong, G.; Armstrong, A. R.; Bruce, P. G.; Reale, P.; Scrosati, B. TiO_2(B) nanowires as an improved anode material for lithium-ion batteries containing $LiFePO_4$ or $LiNi_{0.5}Mn_{1.5}O_4$ cathodes and a polymer electrolyte. *Adv. Mater.* **2006**, *18*, 2597–2600.

[40] Hassoun, J.; Lee, K. S.; Sun, Y. K.; Scrosati, B. An advanced lithium ion battery based on high performance electrode materials. *J. Am. Chem. Soc.* **2011**, *133*, 3139–3143.